JACS
JOURNAL OF THE AMERICAN CHEMICAL SOCIETY
Article
pubs.acs.org/JACS

Photocrystallographic Observation of Halide-Bridged Intermediates in Halogen Photoeliminations

David C. Powers,[†] Bryce L. Anderson,[†] Seung Jun Hwang,[†] Tamara M. Powers,[†] Lisa M. Pérez,[‡] Michael B. Hall,[‡] Shao-Liang Zheng,[†] Yu-Sheng Chen,[§] and Daniel G. Nocera*[,†]

[†]Department of Chemistry and Chemical Biology, Harvard University, 12 Oxford Street, Cambridge, Massachusetts 02138, United States

[‡]Department of Chemistry, Texas A&M University, College Station, Texas 77843, United States

[§]ChemMatCARS, The University of Chicago, Argonne, Illinois 60439, United States

Supporting Information

ABSTRACT: Polynuclear transition metal complexes, which frequently constitute the active sites of both biological and chemical catalysts, provide access to unique chemical transformations that are derived from metal−metal cooperation. Reductive elimination via ligand-bridged binuclear intermediates from bimetallic cores is one mechanism by which metals may cooperate during catalysis. We have established families of Rh_2 complexes that participate in HX-splitting photocatalysis in which metal−metal cooperation is credited with the ability to achieve multielectron photochemical reactions in preference to single-electron transformations. Nanosecond-resolved transient absorption spectroscopy, steady-state photocrystallography, and computational modeling have allowed direct observation and characterization of Cl-bridged intermediates (intramolecular analogues of classical ligand-bridged intermediates in binuclear eliminations) in halogen elimination reactions. On the basis of these observations, a new class of Rh_2 complexes, supported by CO ligands, has been prepared, allowing for the isolation and independent characterization of the proposed halide-bridged intermediates. Direct observation of halide-bridged structures establishes binuclear reductive elimination as a viable mechanism for photogenerating energetic bonds.

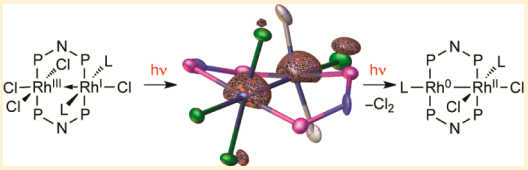

INTRODUCTION

Polynuclear transition metal sites commonly comprise redox catalysts in biological and chemical settings. In Nature, multielectron redox transformations, such as O_2 and H^+ reduction,[1,2] H_2O oxidation,[3] and N_2 fixation,[4] are carried out at polynuclear metal cofactors.[5] In heterogeneous catalysis, high-nuclearity surface features, such as step edges and defects that are capable of interacting with substrates via multipoint binding, are often proposed as catalyst active sites.[6−9] With the aim to harness the potential of multiple reaction centers in proximity to accomplish multielectron chemical transformations, synthetic chemists have targeted development of specific ligand-supported multinuclear catalyst sites.[10−12]

Accomplishing small molecule activation reactions relevant to energy conversion schemes mandates development of catalysis of multielectron, multiproton reactions. We have been particularly interested in development of HX-splitting photocatalysis, which, like H_2O-splitting schemes, stores substantial energy but has the advantage that only two proton/electron equivalents need to be managed to accomplish a closed photocycle in contrast to the four implicit in H_2O splitting.[3,13,14] In this context, we have developed a family of two-electron mixed-valent dirhodium HX-splitting photocatalysts (i.e., Rh_2[I,III] complex **1**, Figure 1) predicated on the hypothesis that two-electron mixed valency can engender molecular excited states with the proclivity to engage in two-electron redox transformations.[15,16] These complexes have proven to be adept at multielectron photoreactions; H_2-

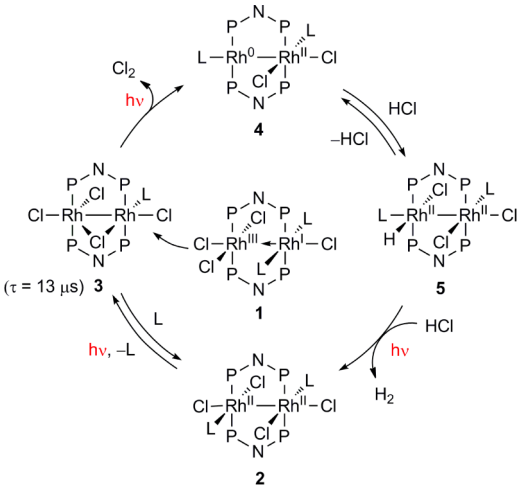

Figure 1. HX-splitting photocycle catalyzed by Rh_2[I,III] complex **1** or Rh_2[II,II] complex **2** involves both proton reduction and halide oxidation. The critical halide oxidation step is proposed to proceed from halide-bridged intermediate **3**.

Received: August 10, 2014
Published: September 29, 2014

   dx.doi.org/10.1021/ja508218v | J. Am. Chem. Soc. 2014, 136, 15346−15355

Table 1. Crystal Data and Structure Refinement

	3	6·THF	*trans*-7	8	9·Et_3NHCl
formula	$C_{29}H_{37}Cl_4F_{24}N_3O_8P_4Rh_2$	$C_{24}H_{28}Cl_2F_{24}N_2O_{11}P_4Rh_2$	$C_{20}H_{22}Cl_4F_{24}N_2O_{10}P_4Rh_2$	$C_{19}H_{22}Cl_4F_{24}N_2O_9P_4Rh_2$	$C_{25}H_{17}Cl_3F_{24}N_3O_9P_4Rh_2$
CCDC no.	1008080	1006061	1006063	1006064	1006060
fw, g/mol	1483.12	1377.51	1377.90	1349.07	1415.05
temp, K	100 (2)	100 (2)	100 (2)	100 (2)	100 (2)
cryst system	triclinic	monoclinic	monoclinic	triclinic	tetragonal
space group	$P\bar{1}$	$C2/m$	$C2/c$	$P\bar{1}$	$I4_1cd$
color	yellow	orange	orange	orange	orange
a, Å	10.2286 (8)	32.468 (6)	23.308 (1)	12.2293 (7)	23.271 (1)
b, Å	12.356 (1)	21.017 (4)	23.326 (1)	18.579 (1)	23.271 (1)
c, Å	20.409 (2)	14.625 (3)	16.9357 (7)	19.257 (1)	36.041 (2)
α, deg	94.387 (1)	90	90	89.993 (1)	90
β, deg	96.782 (1)	114.336 (2)	107.939 (1)	87.029 (1)	90
γ, deg	99.181 (1)	90	90	87.275 (1)	90
V, A^3	2516.5 (3)	9093 (3)	8760.2 (6)	4364.3 (5)	19517 (2)
Z	4	12	8	6	24
R1[a]	0.059	0.087	0.070	0.061	0.033
wR2[b]	0.116	0.267	0.211	0.151	0.072
GOF[c] (F^2)	1.00	1.07	1.03	1.00	1.04
R_{int}	0.095	0.094	0.066	0.118	0.100

[a] $R1 = \sum||F_o| - |F_c||/\sum|F_o|$. [b] $wR2 = (\sum(w(F_o^2 - F_c^2)^2)/\sum(w(F_o^2)^2))^{1/2}$. [c] $GOF = (\sum w(F_o^2 - F_c^2)^2/(n-p))^{1/2}$, where n is the number of data and p is the number of parameters refined.

evolving photocatalysis has been realized in which formal halogen elimination reactions close the catalytic cycle.[17,18]

The challenge in developing HX-splitting chemistry is the halogen elimination half reaction, which has been the bottleneck to development of HX-splitting photochemistry. Only recently has mechanistic information regarding this reaction from dirhodium complexes become available. Nanosecond-resolved transient absorption (TA) spectroscopy of halogen photoelimination reactions from a pair of valence isomers, two-electron mixed-valent complex **1** and valence-symmetric complex **2**, revealed photoelimination via a common intermediate. We proposed this intermediate to be Cl-bridged binuclear complex **3**, generated by photoextrusion of an isocyanide ligand (L, Figure 1) and migration of a Cl ligand to a bridging position.[19] Intermediate **3** represents an intramolecular analogue of ligand-bridged intermediates proposed in binuclear elimination reactions.[20,21]

We now utilize photocrystallography to provide direct information regarding structural changes associated with intermediates of consequence to halogen elimination. Together with solution-phase and solid-state transient absorption and DFT modeling, we establish that halide-bridged intermediates are the critical intermediates of halogen elimination from two-electron bimetallic cores. Complementary synthesis of a new suite of dirhodium complexes allowed isolation and independent evaluation of the chemistry of the halide-bridged bimetallic complexes. Direct observation of halide-bridged structures establishes binuclear reductive elimination as a critical pathway for metal-halide bond activation.

EXPERIMENTAL SECTION

General Considerations. All reactions were carried out in an N_2-filled glovebox. Anhydrous solvents were obtained from drying columns.[22] $[Rh(cod)Cl]_2$ and $[Rh(CO)_2Cl]_2$ were obtained from Strem Chemicals and used without purification. Ligand tfepma,[23] Rh_2[I,III] complex **1**,[19] and Rh_2[II,II] complex **2**[24] were prepared as previously described.

Physical Methods. NMR spectra were recorded at the Harvard University Department of Chemistry and Chemical Biology NMR facility on a Varian Mercury 400 spectrometer operating at 400 MHz for ^1H acquisitions, 162 MHz for ^{31}P acquisitions, and 375 MHz for ^{19}F acquisitions. NMR chemical shifts are reported in ppm, with the residual solvent resonance as internal standard. UV−vis spectra were recorded at 293 K in quartz cuvettes on a Spectral Instruments 400 series diode array blanked against the appropriate solvent. IR spectra were recorded with powdered samples on a PerkinElmer Spectrum 400 FT-IR/FT-FIR spectrometer outfitted with a Pike Technologies GladiATR attenuated total reflectance accessory with a monolithic diamond stage and pressure clamp.

Photochemistry. Steady-state photochemical reactions were performed using a 1000 W high-pressure Hg/Xe arc lamp (Oriel), and the beam was passed through a water-jacketed filter holder containing the appropriate long-pass filter, an iris, and a collimating lens. Samples were photolyzed in a constant-temperature circulating water bath (23 °C). Nanosecond transient absorption (TA) measurements were made using a previously described home-built system.[25] Solution-phase TA measurements were performed on THF solutions of **1** and **2**, and solid-state TA measurements were performed on samples prepared by drop-casting solutions of **1** and **2** (from either CH_2Cl_2 or THF) on glass slides and allowing them to dry under ambient conditions for 1 h. All TA measurements were carried out at 23 °C.

X-ray Crystallographic Details. X-ray structures of complexes **3** and **6**−**10** and variable-temperature (VT) X-ray data were collected on a Bruker three-circle platform goniometer equipped with an Apex II CCD and an Oxford cryostream cooling device operating between 100 and 275 K. Radiation was from a graphite fine focus sealed tube Mo Kα (0.71073 Å) source. Crystals were mounted on a glass fiber pin using Paratone N oil. Data was collected as a series of φ and/or ω scans. Data was integrated using SAINT and scaled with multiscan absorption correction using SADABS.[26] The structures were solved by intrinsic phasing using SHELXT (Apex2 program suite, v2014.1) and refined against F^2 on all data by full matrix least-squares with SHELXL-97.[27] All non-hydrogen atoms were refined anisotropically. H atoms were placed at idealized positions and refined using a riding model. Crystal data and refinement statistics are summarized in Tables 1 and S1, and thermal ellipsoid plots are collected in Figures 5, 7, and S15. Powder diffraction experiments were carried out with a Bruker D2 Phaser using a Cu anode.

Photocrystallography data was collected using 0.41328 Å radiation at temperature of 15 K (Oxford Diffraction Helijet) on a vertical

dx.doi.org/10.1021/ja508218v | J. Am. Chem. Soc. 2014, 136, 15346−15355

mounted Bruker D8 three-circle platform goniometer equipped with an Apex II CCD at ChemMatCARS located at the Advanced Photon Source (APS), Argonne National Laboratory (ANL). Illumination was provided by a Thorlabs 365 nm LED (M365L2) and was delivered to the sample via a 100 μm i.d. fiber optic. Dark structures were solved and refined as described above. For data sets obtained during irradiation, non-H atoms of the product were located in difference-Fourier maps, calculated with coefficients F_0(irradiated) − F_0(dark), and then refined with constraints on the product molecule's atomic displacement parameters to the corresponding values of the reactant molecule (EADP instructions of SHELXL97). The percentage of the reactant in the crystal was treated as a variable in the refinements.

Computational Details. B3LYP[28−30] calculations were performed using the Gaussian 09, revision D.01, suite of software.[31] Model complexes in which adamantyl isocyanide ligand was replaced with a methyl isocyanide and the bridging tfepma ligands were replaced with bis(fluoromethoxyphosphino)methylamine (fmpma) ligands were used in all computations. These model structures are less severe truncations than have previously been employed in computational investigations of phosphazane bridged dirhodium complexes.[32−34] Gas-phase geometry optimizations and TD-DFT calculations were carried out using an SDD basis set for Rh[35] and 6-31G* for all other atoms.[36,37] Stationary points were characterized with frequency calculations. Single-point solvent corrections (THF) were carried out using a polarizable continuum model using the integral equation formalism variant. B3LYP geometries well reproduced experimental metrical parameters, obtained by X-ray crystallography (tabulated in Tables S6 and S7), and provided similar structural parameters as optimizations carried out with either the M06[38,39] or M06-L[40] functional. Computed absorption spectra (line broadening 0.15 eV) reproduced experimental absorption spectra. NBO calculations[41−44] were carried out using Gaussian NBO, version 3.1.[45]

Rh_2(tfepma)$_2$(CO)$_2$Cl$_2$ (6). To a solution of $[Rh(CO)_2Cl]_2$ (38.0 mg, 9.77×10^{-5} mol, 1.00 equiv) in THF (3 mL) at 23 °C was added tfepma (95.2 mg, 1.95×10^{-4} mol, 2.00 equiv) dropwise as a THF (2 mL) solution. The reaction mixture was stirred at 23 °C for 1 h, during which time evolution of bubbles was observed and the color of the reaction mixture turned from orange to dark red. Complex **6** was not isolated as a solid because removal of solvent led to a mixture of Rh_2(tfepma)$_2$(CO)$_2$Cl$_2$ (**6**) and Rh_2(tfepma)$_2$(μ-CO)Cl$_2$ (**9**) and thus solution characterization (^{1}H NMR, ^{19}F NMR, ^{31}P NMR, and UV−vis) was carried out using the reaction solution without further purification. On the basis of integration of the ^{1}H NMR spectrum against hexamethylbenzene (internal standard), the yield of **6** was 98%. ^{1}H NMR (THF-d_8, 23 °C): δ 4.96−4.88 (m, 4H), 4.84−4.74 (m, 12H), 2.99 (pseudoquintet, J = 3.6 Hz, 6H). ^{31}P NMR (THF-d_8, 23 °C): δ 131.2−130.2 (m, 4P). ^{19}F NMR (THF-d_8, 23 °C): δ −75.5 (dt, J = 19.7 Hz, J = 9.2 Hz, 24F). IR: ν_{CN} = 2002 cm^{-1}. Crystals suitable for single-crystal diffraction analysis were obtained from a THF solution layered with pentane at −30 °C. Satisfactory combustion analysis could not be obtained because **6** was not stable to evacuation of solvent.

Rh_2(tfepma)$_2$(CO)$_2$Cl$_4$ (7). To a solution of $[Rh(CO)_2Cl]_2$ (44.0 mg, 1.13×10^{-4} mol, 1.00 equiv) in $PhCH_3$ (5 mL) at 23 °C was added tfepma (110 mg, 2.26×10^{-4} mol, 2.00 equiv) dropwise as a $PhCH_3$ (1 mL) solution. The reaction mixture was stirred at 23 °C for 1 h, during which time evolution of bubbles was observed and the color of the reaction mixture turned from orange to dark red. $PhICl_2$ (46.6 mg, 1.70×10^{-4} mol, 1.50 equiv) was added as a solid. ^{31}P NMR analysis of an aliquot of the reaction mixture showed the presence of two ^{31}P NMR signals (multiplets at 105.3−104.5 and 102.2−101.5 ppm) in a 2:1 ratio, assigned as *trans*-**7** and *cis*-**7**, respectively (Figure S6). Heating the reaction mixture at 70 °C for 2 h resulted in the conversion of *trans*-**7** to *cis*-**7**. The reaction mixture was cooled to −30 °C for 1 h, at which time a precipitate was observed. The solvent was decanted, and the residue washed with pentane and dried in vacuo to afford 123 mg of the title complex as a yellow solid in 79% yield. *trans*-**7**: ^{1}H NMR (C_6D_6, 23 °C): δ 4.86−4.83 (m, 8H), 4.51−4.46 (m, 4H), 4.36−4.31 (m, 4H), 2.58 (pseudoquintet, J = 3.9 Hz, 6H). ^{31}P NMR (C_6D_6, 23 °C): δ 105.3−104.5 (m, 4P). ^{19}F NMR (C_6D_6, 23 °C): δ −74.68 (t, J = 7.9 Hz, 12F), −75.09 (t, J = 7.9 Hz, 12F). IR: ν_{CN} = 2082 cm^{-1}. Crystals of *cis*-**7** suitable for single-crystal diffraction analysis were obtained from a THF solution layered with pentane at −30 °C (see the Supporting Information), and crystals of *trans*-**7** suitable for single-crystal diffraction analysis were obtained from a CH_2Cl_2 solution layered with hexane at −30 °C.

Rh_2(tfepma)$_2$(CO)(μ-Cl)Cl$_3$ (8). A thin film of *trans*-**7** (47.0 mg, 3.41×10^{-4} mol, 1.00 equiv) was deposited on the wall of a two-chamber photoreaction vessel and dried in vacuo for 12 h. Broad-band photolysis of the thin film with a 1000 W Hg lamp was carried out for 4 h under dynamic vacuum (20 mTorr). The residue was taken up in CH_2Cl_2, layered with pentane, and cooled to −30 °C for 1 h, at which time the solvent was decanted. The residue was dried in vacuo to afford 40.1 mg of the title complex as a yellow solid in 87% yield. ^{1}H NMR (C_6D_6, 23 °C): δ 5.02−4.92 (m, 2H), 4.72−4.64 (m, 2H), 4.56−4.46 (m, 4H), 4.45−4.39 (m, 2H), 4.29−4.15 (m, 6H), 2.61 (pseudoquintet, J = 3.9 Hz, 6H). ^{31}P NMR (C_6D_6, 23 °C): δ 106.8−104.2 (m, 4P). ^{19}F NMR (C_6D_6, 23 °C): δ −74.49 (t, J = 7.9 Hz, 6F), −74.90 (t, J = 7.9 Hz, 6F), −74.92 (t, J = 7.9 Hz, 6F), −75.08 (t, J = 7.9 Hz, 6F). IR: ν_{CN} = 2086 cm^{-1}. Crystals of **8** suitable for single-crystal diffraction analysis were obtained from a THF solution layered with pentane at −30 °C.

Rh_2(tfepma)$_2$(μ-CO)Cl$_2$ (9). To a solution of $[Rh(CO)_2Cl]_2$ (63.7 mg, 1.64×10^{-4} mol, 1.00 equiv) in THF (5 mL) at 23 °C was added tfepma (160 mg, 3.28×10^{-4} mol, 2.00 equiv) dropwise as a THF (5 mL) solution. The reaction mixture was stirred at 23 °C for 1 h, during which time evolution of bubbles was observed and the color of the reaction mixture turned from orange to dark red. The solvent was removed in vacuo. The residue was dissolved in CH_2Cl_2 (5 mL), and the solvent was removed in vacuo. The redissolution/evaporation sequence was repeated four times, and the residue was triturated in pentane to afford 176 mg of complex **9** as an orange solid (84% yield). ^{1}H NMR (CD_2Cl_2, 23 °C): δ 4.70−4.60 (m, 8H), 4.59−4.47 (m, 8H), 2.75 (pseudoquintet, J = 3.5 Hz, 6H). ^{31}P NMR (CD_2Cl_2, 23 °C): δ 130.1−129.1 (m, 4P). ^{19}F NMR (CD_2Cl_2, 23 °C): δ −75.3 (br s, 24F). IR: ν_{CN} = 1812 cm^{-1}. Combustion analysis, found (calcd): C, 17.95 (17.84); H, 1.96 (1.73); N, 2.17 (2.19). Crystals suitable for single-crystal diffraction analysis were obtained from a THF solution **9** and Et_3NHCl layered with pentane at −30 °C.

Rh_2(tfepma)$_2$(CO)(AdNC)Cl$_4$ (10). To a solution of Rh_2(tfepma)$_2$(μ-CO)Cl$_2$ (**9**) (120 mg, 9.40×10^{-5} mol, 1.00 equiv) in THF (2 mL) at 23 °C was added AdNC (15.2 mg, 9.40×10^{-5} mol, 1.00 equiv) dropwise as a THF (1 mL) solution. The reaction mixture was stirred at 23 °C for 30 min, and the solvent was removed in vacuo. The residue was taken up in CH_2Cl_2 (2 mL), and $PhICl_2$ (28.4 mg, 1.03×10^{-4} mol, 1.10 equiv) was added. Hexanes (15 mL) were added, and the reaction mixture was cooled to −30 °C for 12 h, at which time 75.3 mg of complex **10** was isolated as an orange crystalline solid (53% yield). ^{1}H NMR (CD_2Cl_2, 23 °C): δ 5.22−5.14 (m, 4H), 4.83−4.68 (m, 8H), 4.65−4.55 (m, 4H), 3.02 (pseudoquintet, J = 3.9 Hz, 6H), 2.25 (br s, 3H), 2.18 (br s, 6H), 1.80 = 1.71 (m, 6H). ^{31}P NMR (CD_2Cl_2, 23 °C): δ 113.6−111.1 (m, 2P), 108.4−106.7 (m, 2P). ^{19}F NMR (CD_2Cl_2, 23 °C): δ −75.3 (t, J = 7.9 Hz, 6F), −75.4 (t, J = 7.9 Hz, 6F), −75.5 (t, J = 7.9 Hz, 6F), −75.8 (t, J = 7.8 Hz, 6F). IR: ν_{CN} = 2193 cm^{-1}, 2093 cm^{-1}. Crystals suitable for single-crystal diffraction analysis were obtained from a CH_2Cl_2 solution of **10** layered with hexanes at −30 °C.

Rh_2(tfepma)$_2$AdNC(μ-Cl)Cl$_3$ (3). A thin film of *trans*-**7** (52.0 mg, 3.44×10^{-4} mol, 1.00 equiv) was deposited on the wall of a two-chamber photoreaction vessel and dried in vacuo for 12 h. Broad-band photolysis of the thin film with a 1000 W Hg lamp was carried out for 4 h under dynamic vacuum (20 mTorr). The residue was taken up in CH_2Cl_2, layered with pentane, and cooled to −30 °C for 1 h, at which time the solvent was decanted. The residue was dried in vacuo to afford 48.0 mg of complex **3** as a yellow solid (94% yield). ^{1}H NMR (CD_2Cl_2, 23 °C): δ 4.93−4.83 (m, 4H), 4.82−4.67 (m, 6H), 4.62−4.54 (m, 2H), 4.51−4.45 (m, 2H), 4.36−4.27 (m, 2H), 3.02 (pseudoquintet, J = 3.9 Hz, 6H), 2.13 (br s, 3H), 2.09 (s, 6H), 1.72−1.64 (m, 6H). ^{31}P NMR (CD_2Cl_2, 23 °C): δ 116.5−114.4 (m, 2P), 113.2−111.1 (m, 2P). ^{19}F NMR (C_6D_6, 23 °C): δ −74.64 (t, J =

dx.doi.org/10.1021/ja508218v | J. Am. Chem. Soc. 2014, 136, 15346−15355

7.9 Hz, 6F), −75.30 to −75.4 (m, 18F). IR: ν_{CN} = 2199 cm^{-1}. Crystals of **3** suitable for single-crystal diffraction analysis were obtained by cooling a saturated CH_2Cl_2/hexanes solution of **3** to −30 °C.

RESULTS

Photocrystallography. Thin-film TA spectroscopy was used to establish the homology of solution-phase and solid-state photoreactions. Thin films of complexes **1** and **2**, drop-cast from either THF or CH_2Cl_2 solutions, showed UV−vis absorption spectra that overlaid with solution spectra of **1** and **2** (Figure S24). The thin films are polycrystalline based on powder X-ray diffraction (**1**, Figure S22; **2**, Figure S23), but the crystal phase could not be established due to anisotropic orientation of crystallites, which is typical of polycrystalline thin films.[46] TA spectra (λ_{exc} = 355 nm) of these films were recorded at 1 μs delay and show similar features to those observed in solution-phase TA spectra of these complexes, confirming the formation of the same photointermediate in both solution and solid state (Figure 2).

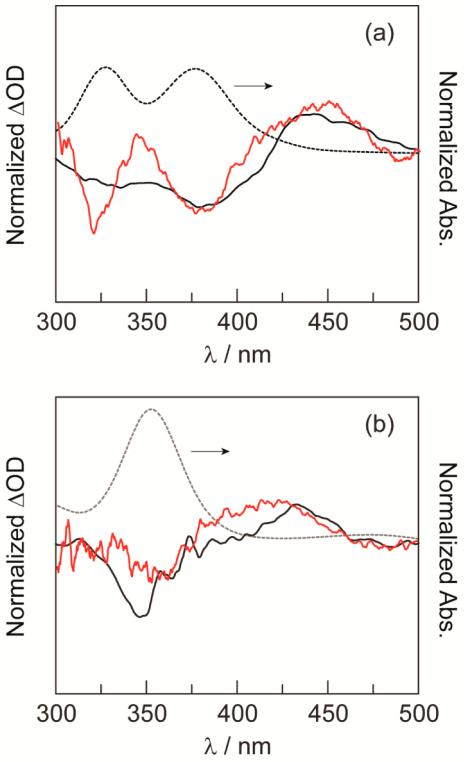

Figure 2. UV−vis spectra (dotted black), solution-phase TA spectra (solid black), and thin-film TA spectra (red) of (a) Rh_2[I,III] complex **1** and (b) Rh_2[II,II] complex **2**. TA spectra were obtained by flash laser photolysis (355 nm) and recorded at a 1 μs delay.

Steady-state photocrystallography experiments were performed at the Advanced Photon Source (APS) housed at Argonne National Laboratory (ANL) using synchrotron radiation (0.41328 Å) and a 365 nm LED light source (5 mW power measured at the crystal). A photodifference map was generated by comparing diffraction data obtained for a single crystal of Rh_2[I,III] complex **1** in the dark with diffraction data obtained for the same crystal during irradiation (Figure 3a). The crystal was not moved between the acquisitions of the two data sets and thus the orientation matrix was unchanged during the experiment. The difference map showed the

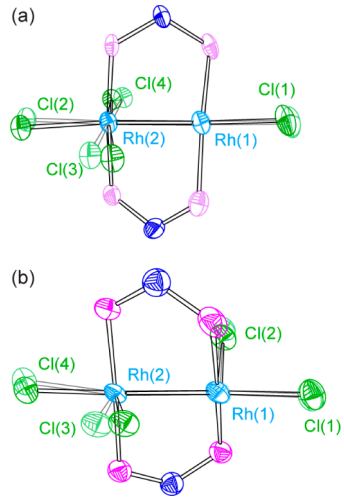

Figure 3. Thermal ellipsoid plots of photocrystallography results with photoinduced structures (solid) superimposed on dark structures (faded). (a) Rh_2[I,III] plot; Rh^1−Rh^2−Cl^3 91.05(5)° (dark), 83.2(2)° (photoinduced). (b) Rh_2[II,II] plot; Rh^1−Rh^2−Cl^3 91.15(5)° (dark), 78(2)° (photoinduced).

presence of a photoinduced structure populated at 5.7(9)% of the crystal. Examination of the structural perturbations in the photoinduced structure shows ligand reorganization that would be anticipated during a migration of one of the chloride ligands to a bridging position; key metrics include the Rh^1−Rh^2−Cl^3 bond angle, which contracts from 91.05(5) to 83.2(2)° in the photoinduced structure. Concurrent with this, Rh^1−Rh^2−Cl^4 expands from 90.97(5) to 92(2)°. Additionally, Rh^2−Cl^3, which is the bond vector participating in partial migration from terminal to bridging coordination mode, elongates from 2.362(2) to 2.66(4) Å (additional metrical parameters are provided in Table S4).

The extent of laser heating of the sample during data acquisition was examined by comparing the size of thermal ellipsoids of atoms not involved in the primary photoreaction (i.e., *N*-atoms in the phosphazane ligand) with the size of thermal ellipsoids for the same atoms as a function of temperature.[47] On the basis of this analysis, laser heating warmed the single crystal of **1** from 15 to ∼250 K (Figure S18). The metrical parameters of **1** do not show significant temperature-dependent variation (Table S2), confirming that the difference map arises from photochemical, not thermal, effects.

The photoinduced structure derived from complex **1** was accessed rapidly during irradiation. Comparison of specific reflections from the structures obtained in the dark and under illumination revealed a set of reflections that showed substantial intensity changes upon irradiation. Examination of these particular reflections as the light was turned on showed that the intensity changes as a step function: the intensity increased rapidly relative to data collection and then reaches a steady-state value during irradiation (Figure S19).

A steady-state photocrystallography experiment was also performed using a single crystal of Rh_2[II,II] complex **2** under identical conditions as those of the aforementioned experiment with **1** (15 K, 5 mW 365 nm irradiation, 0.41328 Å synchrotron radiation). A photoinduced structure was identified in the photodifference map in which the Rh^1−Rh^2−Cl^3 angle contracts from 91.15(5) to 78(2)° upon irradiation (Figure 3b). Partial migration of Cl^3 toward the bridging position is

dx.doi.org/10.1021/ja508218v | J. Am. Chem. Soc. 2014, 136, 15346−15355

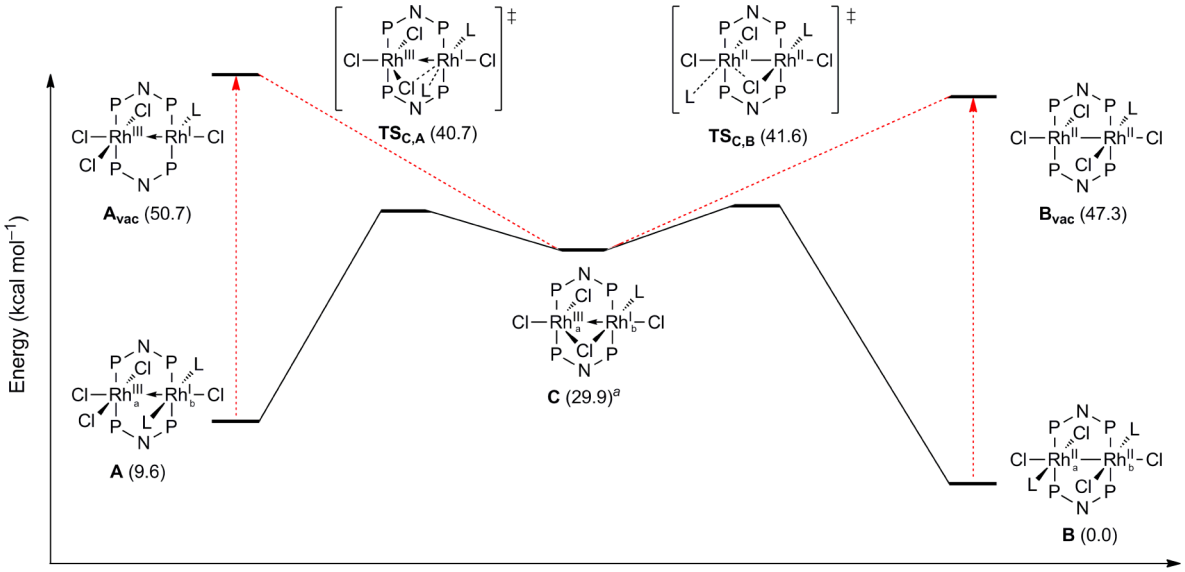

Figure 4. Calculated gas-phase stationary points in the interconversions of Rh_2 structures **A**–**C**. Site-vacant complexes $\mathbf{A}_{vac}$ and $\mathbf{B}_{vac}$ were evaluated by single-point calculations. Energies are solvent-corrected electronic energies at 0 K. [a]Sum of E_0(**C**) and E_0(MeNC).

accompanied by substantial elongation of the Rh–Cl bond (2.378(2) to 2.57(8) Å). The photoinduced geometry could be identified in the photodifference map generated from **2**, but full-molecule disorder in the available single crystals of **2** precluded determination of the population of the photoinduced structure. Variable-temperature crystallography experiments performed on a single crystal of **2** confirm that the observed structural effects are photoinduced, not thermally promoted. Similar to experiments carried out with complex **2**, the photoinduced structure is accessed rapidly relative to data acquisition. Upon cessation of irradiation, the photoinduced structure is no longer observed in the photodifference map, indicating that the photoinduced state is accessed only during steady-state irradiation.

Computational Results. Natural bond order (NBO) calculations were undertaken to evaluate the electronic structure of the dirhodium complexes investigated in this study. Herein, computed structures are referred to by letter, not compound numbers (i.e., **A** is the computed structure of **1**). In each of **A**, **B**, and **C** (i.e., computed structures of **1**, **2**, and **3**, respectively), the highest-occupied NBO is Rh–Rh bonding. The Rh–Rh bond in **A** is polarized, as would be expected of a dative bond between a d^6 and a d^8 metal (Rh_a/Rh_b = 38.5:61.5). For valence symmetric Rh_2[II,II] structure **B**, the Rh–Rh bond is symmetrically shared by the two Rh atoms (Rh_a/Rh_b = 51.3:48.7). Consistent with a two-electron mixed-valent formulation, the M–M bond of structure **C** is polarized to a similar extent as that of the M–M bond in **A** (Rh_a/Rh_b = 42.6:57.4), consistent with the bonding predictions of the covalent bond classification for a dative covalent bond between the Rh centers.[48,49]

Density functional theory (DFT) calculations, summarized in Figure 4, address the structural manifestations of complete dissociation of one isocyanide ligand, as would be anticipated in the solution phase where free diffusion of the dissociated ligand is expected. Removal of one isocyanide ligand from either Rh_2[I,III] structure **A** or Rh_2[II,II] structure **B** results in site-vacant structures $\mathbf{A}_{vac}$ and $\mathbf{B}_{vac}$, respectively. Structures $\mathbf{A}_{vac}$ and $\mathbf{B}_{vac}$ were evaluated with single-point calculations because neither could be located as a stationary point; both $\mathbf{A}_{vac}$ and $\mathbf{B}_{vac}$ evolved to structure **C** without a barrier (Figures S31 and S32). Reaction of photoextruded isocyanide ligand with chloride-bridged structure **C** could proceed at Rh_b to regenerate Rh_2[I,III] complex **A** or at Rh_a to accomplish photoisomization to Rh_2[II,II] complex **B**. The computed relative transition state energies for conversion of **C** to **A** and **C** to **B** are 10.8 and 11.7 kcal/mol, respectively. Consistent with these calculations, complex **1** displays wavelength-dependent photochemistry, undergoing both photoreduction (λ_{exc} > 295 nm) and photoisomerization (λ_{exc} > 380 nm) reactions. Both isomerization and photoreduction reactions proceed via a common intermediate; identical TA spectral line shapes were obtained when samples of Rh_2 complex **1** underwent laser flash photolysis with either 355 or 385 nm incident light (Figure S30).

As opposed to solution photochemistry, free ligand dissociation during photocrystallography experiments is not possible because ligand motions are constrained by the crystal matrix.[50] To probe the impact of restricted isocyanide ligand dissociation, the geometry of Rh_2[I,III] structure **A** was evaluated as a function of M–L bond length. The results are tabulated in Table 2 and show that small perturbations of the

Table 2. Computed Bond Metrics as a Function of M–L Distance

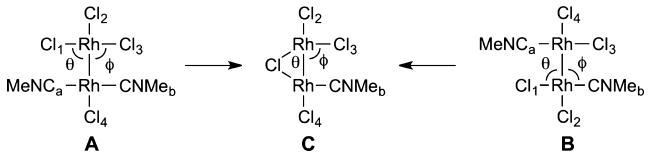

$Rh–L_a$ (Å)	θ (deg)	ϕ (deg)	$Rh–L_a$ (Å)	θ (deg)	ϕ (deg)
1.99 (**A**)	89.99	94.05	1.93 (**B**)	90.80	91.97
2.20	89.25	94.60	2.20	90.39	92.81
2.46	88.10	95.40	2.46	89.49	93.61
2.70	86.62	96.40	2.70	88.43	94.12
2.90	84.12	97.94	2.90	86.51	95.21
3.15	78.91	100.85	3.15	81.25	97.17
∞ (**C**)	58.16	101.13	∞ (**C**)	58.16	101.13

dx.doi.org/10.1021/ja508218v | J. Am. Chem. Soc. 2014, 136, 15346–15355

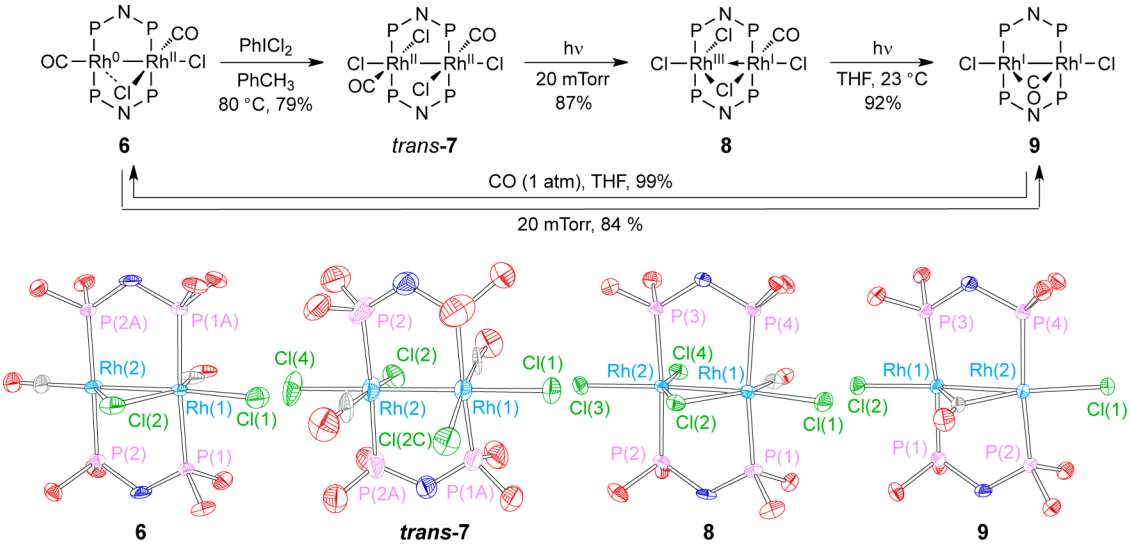

Figure 5. Synthesis of a suite of Rh_2 carbonyl complexes. Thermal ellipsoid plots of **6**–**9** in which solvent molecules, H atoms, and $-CH_2CF_3$ groups have been removed for clarity. Ellipsoids are drawn at 50% probability.

M–L bond length are sufficient to induce nascent migration of a proximal Cl ligand toward a bridging position. Similar M–L bond-length-dependent migrations were computed starting with Rh_2[II,II] structure **B**. TD-DFT calculations of both **A** and **B** as a function of M–L bond length show that even partial migration of a Cl ligand toward a bridging site begins to give rise to the spectral features observed in thin-film TA measurements of both **1** and **2** (Figure S39). Analogous results, both regarding free diffusion as would be encountered in solution and restricted diffusion as would be encountered in the solid state, have been obtained for homologous series of CO complexes (summarized in the Supporting Information).

Synthesis and Photochemistry of Dirhodium Carbonyls. To evaluate the hypothesis that complete ligand rearrangement to a Cl-bridged intermediate is impeded in the solid state, a new suite of complexes in which the bulky AdNC ligands of **1** and **2** are replaced with small volatile CO ligands was prepared. The synthetic chemistry and X-ray characterization of these complexes is summarized in Figure 5.

Entry into this suite of Rh_2 carbonyl complexes was gained by treatment of $[Rh(CO)_2Cl]_2$ with tfepma in THF, which resulted in the formation of Rh_2[0,II] carbonyl complex **6** in 98% yield (Figure 5). Two features of **6** are notable. First, the complex displays rapid ligand fluxionality at 23 °C, as evidenced by observation of a single resonance in the ^{31}P NMR spectrum of **6** at 23 °C. Variable-temperature (VT) ^{31}P NMR of **6** between −97 and 23 °C shows that at temperatures below −65 °C two ^{31}P NMR resonances are resolved, consistent with the two-electron mixed-valence formulation indicated by single-crystal X-ray diffraction. Second, one of the carbonyl ligands of **6** is labile. Evaporation of reaction solvent results in isolation of μ-CO–Rh_2[I,I] monocarbonyl complex **9**, the product of CO dissociation.

Treatment of $PhCH_3$ solutions of **6** with $PhICl_2$ results in a mixture of *cis*- and *trans*-**7**. Heating this mixture of Rh_2[II,II] complexes at 80 °C leads to isomerization of *cis*-**7** to *trans*-**7**, which was isolated in 79% yield. *trans*-**7** is an analogue of Rh_2[II,II] complex **2** in which the AdNC ligands of **2** have been replaced by CO ligands. Our contention that complexes supported by volatile ligands would participate in solid-state photochemistry was probed by irradiation of a thin film of *trans*-**7** under vacuum (20 mTorr). Solid-state photolysis led to the expulsion of a CO ligand and the formation of Cl-bridged monocarbonyl complex **8** in 87% yield. Single-crystal X-ray diffraction of the photoproduct confirmed a μ-Cl-Rh_2 geometry for **8**, similar to previously synthesized isocyanide supported Cl-bridged structures.[19] Solution-phase photolysis of *trans*-**7** in THF also led to the rapid conversion to **8**, as established by monitoring the reaction by UV–vis spectroscopy (Figure 6a).

Photolysis of monocarbonyl Rh_2 complex **8** in THF results in the disappearance of the UV–vis features of **8** and the evolution of features attributable to complex **9**, the product of

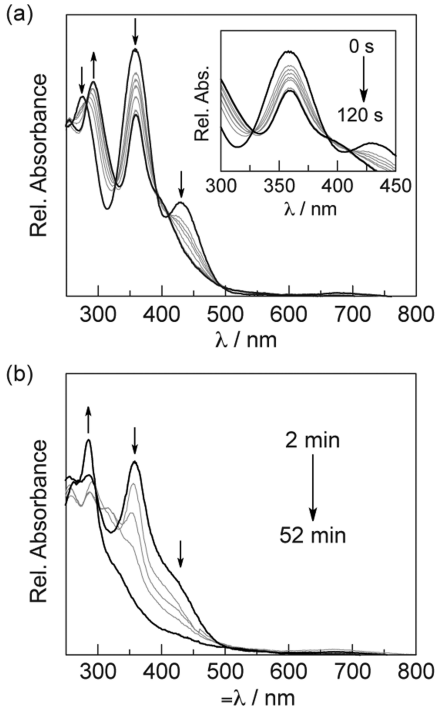

Figure 6. Spectral evolution for the photolysis of *trans*-**7** in THF (λ_{exc} > 305 nm). (a) During the first 120 s, *trans*-**7** is converted to Cl-bridged Rh_2 complex **8**. (b) Subsequently, **8** is converted to Rh_2[I,I] complex **9**, the product of halogen photoelimination.

dx.doi.org/10.1021/ja508218v | J. Am. Chem. Soc. 2014, 136, 15346–15355

two-electron photoreduction (Figure 6b). Complex **9** produced by photolysis of **8** displayed identical spectral features to those of an authentic sample prepared by removal of a CO ligand from complex **6** under vacuum. Monocarbonyl complex **9** is converted to dicarbonyl Rh_2 complex **6** by exposure to 1 atm of CO in 99% yield.

Access to Rh_2 monocarbonyl complex **9** provided an avenue toward synthesis of AdNC-supported μ-Cl-Rh_2 intermediate **3**. Treatment of monocarbonyl complex **9** with 1 equiv of AdNC, followed by oxidation with $PhICl_2$ led to Rh_2[II,II] complex **10**, supported by one AdNC and one CO ligand (Figure 7). Solid-

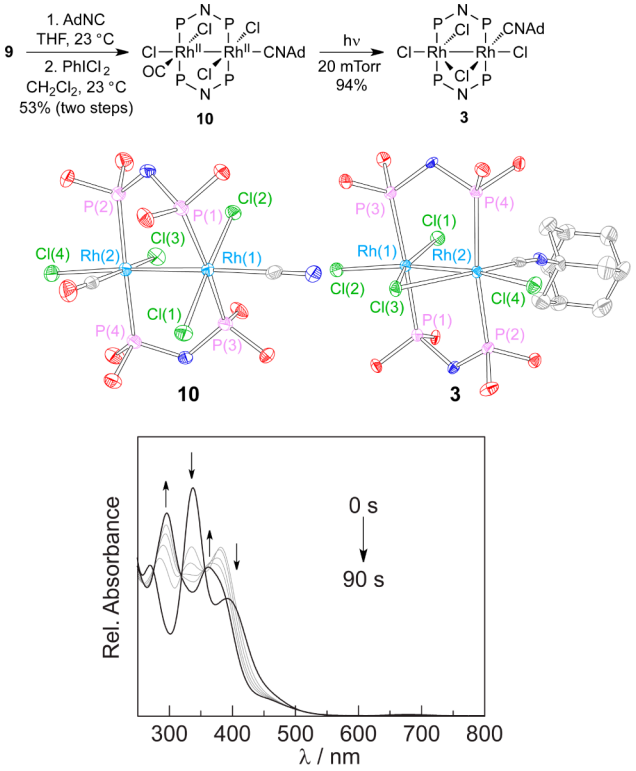

Figure 7. Synthesis of Cl-bridged complex **3** by CO photoextrusion from complex **10**. Thermal ellipsoid plots of **3** and **10** in which H atoms, $-CH_2CF_3$ groups, and adamantyl group from **10** have been omitted for clarity. Ellipsoids are drawn at 50% probability. Spectral evolution for the photolysis of **10** in THF (λ_{exc} > 305 nm) shows conversion to **3** from CO extrusion.

state photolysis of **10** under vacuum led to the expulsion of the CO ligand and isolation of μ-Cl-Rh_2 complex **3**. Prepared from **10**, complex **3** was indefinitely stable and could be independently characterized. Subtraction of the extinction spectra of complexes **1** and **2** from the extinction spectrum measured for **3** confirmed that the photointermediate observed in the TA spectra of **1** and **2** is indeed Cl-bridged complex **3** (Figure 8).

DISCUSSION

Photochemical HX splitting, in which H^+ reduction to H_2 is coupled to X^- oxidation to X_2, offers a paradigm for the construction of a closed, carbon-neutral cycle for solar energy conversion. Halogen elimination accounts for the majority of the energy stored in HX-splitting cycles, and this half-reaction typically has been the roadblock to development of authentic HX-splitting photocatalysis.[16] When halogen elimination is

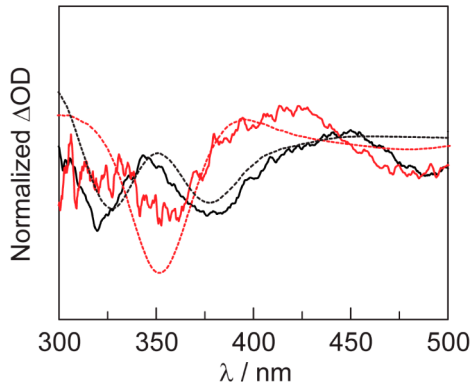

Figure 8. TA spectra (solid) obtained by laser flash photolysis of **1** (black) and **2** (red) thin films (355 nm pump, 1 μs delay). Simulated TA spectra (dotted) obtained by taking the difference of the extinction spectra of **3** with **1** and **2**, respectively.

achieved, chemical traps are frequently required to sequester the evolved halogen.[51−55] The use of chemical traps provides a thermodynamic driving force for photoreduction and obviates significant energy storage. Trap-free halogen elimination chemistry has been realized in the solid state,[57−59] but, as of yet, no system is available for which both proton reduction and solid-state halide oxidation are facile.

Our group has developed dirhodium complexes on the hypothesis that mixed-valent complexes will give rise to the requisite multielectron photoreactions. Families of phosphazane-bridged complexes have been developed, and they display the targeted multielectron chemistry, but catalysts that accomplish authentic HX splitting to afford both H_2 and X_2 in the absence of chemical traps have proven to be elusive. Rational development of new HX-splitting platforms has been limited by a dearth of information regarding the mechanism of halogen elimination, thus establishing an imperative for an understanding of the critical steps preceding halogen elimination.

To this end, the results reported herein provide direct insight into the nature of intermediates that promote halogen elimination from bimetallic centers. Halogen elimination proceeds from a common photointermediate for HX-splitting photocatalysis that is promoted by either Rh_2[I,III] complex **1** or Rh_2[II,II] complex **2**. Solution-phase, nanosecond-resolved TA spectroscopy has provided evidence for this photointermediate, but its structure has not been established.[19] We have employed photocrystallography to directly probe photoinduced structural changes associated with halogen photoelimination by X-ray diffraction.[60−64] Such experiments are particularly attractive given that solid-state halogen elimination reactions provide inroads to authentic halogen elimination reactions.[57−59] To use photocrystallography reliably to gain insight into the structures of reaction intermediates in solution, the same photointermediates must be accessed in the solid state. The thin-film, nanosecond-resolved TA measurements shown in Figure 2 establish the homology of solution-phase and solid-state intermediates; the same TA line shape is generated in solution-phase and solid-state experiments. The nature of this photoreduction intermediate that is common to complexes **1** and **2** is unveiled by the steady-state photocrystallography experiments summarized in Figure 3. Both Rh_2[I,III] complex **1** and Rh_2[II,II] complex **2** display photoinduced structures characteristic of partial halide migration to a bridging position.

dx.doi.org/10.1021/ja508218v | J. Am. Chem. Soc. 2014, 136, 15346−15355

DFT calculations lend support to the structural changes observed by photocrystallography. Specifically, in solution-phase experiments, photodissociated ligands can diffuse away from the transition metal fragment, whereas in the solid state, free diffusion is not possible. Our calculations support the contention that in solution complete dissociation of photoextruded ligands will lead to the formation of chloride-bridged structure **3** (Figure 4). In the solid state, ligand diffusion is constrained and thus, while M−L bond elongation is achievable, complete dissociation is not possible. We modeled this scenario by evaluating the effect of M−L bond elongation of the geometry of the binuclear core and found that at small elongations of the M−L bond partial migration of a chloride ligand toward a bridging configuration was observed (Table 2).

The observation of incomplete ligand migration by photocrystallography emphasizes the rigorous demand of solid-state photoreactions, in which dissociation and diffusion of ligands are not typically possible; the presence of AdNC ligands prevents access to a complete rearrangement to a halide-bridged structure. Management of solid-state ligand inventory was achieved by replacing AdNC ligands with small, volatile CO ligands (Figure 5). This strategy was predicated on the hypothesis that a small, volatile ligand such as CO could be removed as a gas during solid-state photochemistry. Photolysis of *trans*-**7**, an analogue of **2** in which the AdNC ligands are replaced by CO ligands, initially affords chloride-bridged complex **8**, which confirms that photoextrusion of an L-type ligand initially generates a halide-bridged complex (Figure 6a). The halide-bridged complex appears as an intermediate in an interrupted halogen elimination reaction, as further irradiation of **8** led to the isolation of Rh[I,I] complex **9**, which arises from two-electron photoreduction of **8** (Figure 6b).

The two-step reaction sequence, ligand loss to generate a ligand-bridged intermediate followed by two-electron photoreduction, represents an intramolecular example of the two steps of canonical binuclear elimination mechanisms. Binuclear reductive elimination reactions, originally defined in the context of elimination of alkanes and aldehydes from binuclear metal alkyl or acyl complex,[20,21] are proposed to proceed via (1) generation of an open coordination site on the metal alkyl complex by either ligand dissociation or migratory insertion, (2) intermolecular reaction of the unsaturated fragment with a metal hydride to generate a hydride-bridged intermediate, and (3) migration of the alkyl or acyl group onto the bridging hydride to generate the observed organic products as well as binuclear transition metal complexes (eq 1).[65−67] Such binuclear elimination has been proposed for complexes based on most of the transition metal series,[68−72] and it is proposed to be operative during both Co- and Rh-catalyzed hydroformylation reactions under some conditions.[20,73−80] We have previously proposed a binuclear reductive elimination mechanism for the H_2 evolution step of HX-splitting catalysis with phosphazane-bridged Ir_2 complexes.[81]On the basis of the results shown in Figures 2, 3, and 5, we now observe that a similar mechanism may be operative for halogen photoelimination.

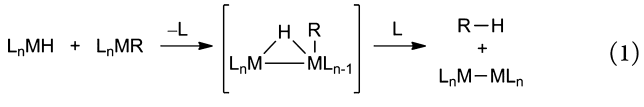

(1)

To firmly establish a binuclear elimination pathway for halogen photoelimination from AdNC-supported complexes **1** and **2**, we sought to directly prepare and characterize the proposed AdNC-supported chloride-bridged intermediate. While preparation by ligand extrusion from either **1** or **2** was judged to be implausible given the short lifetime measured for **3** under these conditions (~15 μs),[19] we anticipated that the complex may be isolable if recombination of the photoextruded ligand with the Rh_2 fragment could be avoided. Taking advantage of the solid-state ligand management enabled with CO ligands, we have prepared and isolated complex **3**, which is the exact transient intermediate that would be generated during halogen elimination from complexes **1** and **2**. We note that chloride-bridged complex **3** is furnished directly by the extrusion of one equivalent of CO upon the solid-state photolysis of **10**, an analogue of **2** in which the Rh_2 core is supported by one AdNC and one CO ligand (Figure 7). With the absorption spectrum of **3** in hand, Figure 8 shows that the TA spectra obtained by laser flash photolysis of **1** or **2** is closely replicated by computing the difference spectra expected based on the experimentally measured ground-state absorption spectra of **1**−**3**.

The confirmed intermediacy of **3** in halogen elimination from **1** and **2** demonstrates that halogen elimination proceeds by a canonical binuclear elimination pathway in which both steps, ligand dissociation to afford a ligand-bridged intermediate and subsequent M−X bond activation, can be directly observed. To our knowledge, the chemistry reported herein is the first instance in which these two steps of binuclear elimination have been directly observed. Photoreduction of **3** may proceed by concerted or stepwise elimination.

The results reported herein offer evidence that X_2 elimination from Rh_2 complexes proceeds via ligand-bridged intermediates, and, accordingly, they inform next-generation catalyst design. Phosphazane-bridged binuclear complexes have been proposed to facilitate ligand rearrangements to ligand-bridged intermediates owing to the ligand's ability to accommodate two-electron changes at the metal core with minimal reorganization energy.[81] The photocrystallography experiments described here support this contention by showing the prevalence of halide-bridged intermediates that preceded M−X bond activation. Although the solid state imposes constraints on the requisite ligand-bridged intermediates, we have leveraged the volatility of carbonyl ligands to allow for the isolation of halide-bridged structures during an interrupted binuclear elimination. This strategy has been exploited to characterize the absorption spectrum of the exact halide-bridged intermediate that is observed transiently (<15 μs) during photocatalysis. Because the solid state offers a mechanism to prevent the back reaction of reactive volatile photoproducts such as X_2, these results suggest that obstacles imposed on photochemical transformations in the solid state might be overcome by clever design of the ligand coordination sphere.

■ ASSOCIATED CONTENT

Supporting Information

Detailed experimental procedures, spectroscopic data for all new compounds, *XYZ* coordinates of computed structures, X-ray crystal data for complex *cis*-**7** and **10**, and complete ref 31. This material is available free of charge via the Internet at http://pubs.acs.org.

■ AUTHOR INFORMATION

Corresponding Author

dnocera@fas.harvard.edu

Notes

The authors declare no competing financial interest.

■ ACKNOWLEDGMENTS

We gratefully acknowledge the NSF for funding (CHE-1332783). D.C.P. is supported by a Ruth L. Kirchenstein National Research Service award (F32GM103211). Photocrystallography was carried out at ChemMatCARS, Sector 15, APS, which is principally supported by the NSF/DOE under grant no. NSF/CHE-1346572. Use of APS was supported by the U.S. DOE, Office of Science, Office of Basic Energy Sciences, under contract no. DE-AC02-06CH11357. Computations were carried out at the Supercomputing Facility and the Laboratory for Molecular Simulation at Texas A&M University.

■ REFERENCES

(1) Ferguson-Miller, S.; Babcock, G. T. *Chem. Rev.* **1996**, *96*, 2889−2907.
(2) Fontecilla-Camps, J. C.; Volbeda, A.; Cavazza, C.; Nicolet, Y. *Chem. Rev.* **2007**, *107*, 4273−4303.
(3) McEvoy, J. P.; Brudvig, G. W. *Chem. Rev.* **2006**, *106*, 4455−4483.
(4) Hoffman, B. M.; Lukoyanov, D.; Yang, Z.-Y.; Dean, D. R.; Seefeldt, L. C. *Chem. Rev.* **2014**, *114*, 4041−4062.
(5) Holm, R. H.; Kennepohl, P.; Solomon, E. I. *Chem. Rev.* **1996**, *96*, 2239−2314.
(6) Dahl, S.; Logadottir, A.; Egeberg, R. C.; Larsen, J. H.; Chorkendorff, I.; Törnqvist, E.; Nørskov, J. K. *Phys. Rev. Lett.* **1999**, *83*, 1814−1817.
(7) Zambelli, T.; Wintterlin, J.; Trost, J.; Ertl, G. *Science* **1996**, *273*, 1688−1690.
(8) Kratzer, P.; Pehlke, E.; Scheffler, M.; Raschke, M. B.; Höfer, U. *Phys. Rev. Lett.* **1998**, *81*, 5596−5599.
(9) Jaramillo, T. F.; Jørgensen, K. P.; Bonde, J.; Nielsen, J. H.; Horch, S.; Chorkendorff, I. *Science* **2007**, *317*, 100−102.
(10) Powers, T. M.; Betley, T. A. *J. Am. Chem. Soc.* **2013**, *135*, 12289−12296.
(11) Krogman, J. P.; Foxman, B. M.; Thomas, C. M. *J. Am. Chem. Soc.* **2011**, *133*, 14582−14585.
(12) Tsui, E. Y.; Kanady, J. S.; Agapie, T. *Inorg. Chem.* **2013**, *52*, 13833−13848.
(13) Cook, T. R.; Dogutan, D. K.; Reece, S. Y.; Surendranath, Y.; Teets, T. S.; Nocera, D. G. *Chem. Rev.* **2010**, *110*, 6474−6502.
(14) Esswein, A. J.; Nocera, D. G. *Chem. Rev.* **2007**, *107*, 4022−4047.
(15) Cotton, F. A.; Nocera, D. G. *Acc. Chem. Res.* **2000**, *33*, 483−490.
(16) Nocera, D. G. *Inorg. Chem.* **2009**, *48*, 10001−10017.
(17) Heyduk, A. F.; Nocera, D. G. *Science* **2001**, *293*, 1639−1641.
(18) Esswein, A. J.; Veige, A. S.; Nocera, D. G. *J. Am. Chem. Soc.* **2005**, *127*, 16641−16651.
(19) Powers, D. C.; Chambers, M. B.; Teets, T. S.; Elgrishi, N.; Anderson, B. L.; Nocera, D. G. *Chem. Sci.* **2013**, *4*, 2880−2885.
(20) Norton, J. R. *Acc. Chem. Res.* **1979**, *12*, 139−145.
(21) Halpern, J. *Inorg. Chim. Acta* **1982**, *62*, 31−37.
(22) Pangborn, A. B.; Giardello, M. A.; Grubbs, R. H.; Rosen, R. K.; Timmers, F. J. *Organometallics* **1996**, *15*, 1518−1520.
(23) Teets, T. S.; Cook, T. R.; Nocera, D. G. *Inorg. Synth.* **2010**, *35*, 164−168.
(24) Elgrishi, N.; Teets, T. S.; Chambers, M. B.; Nocera, D. G. *Chem. Commun.* **2012**, *48*, 9474−9476.
(25) Powers, D. C.; Anderson, B. L.; Nocera, D. G. *J. Am. Chem. Soc.* **2013**, *135*, 18876−18883.
(26) *Apex II*; Bruker AXS: Madison, WI, 2009.
(27) Sheldrick, G. M. *Acta Crystallogr.* **2010**, *D66*, 479−485.
(28) Stephens, P. J.; Devlin, F. J.; Chabalowski, C. F.; Frisch, M. J. *J. Phys. Chem.* **1994**, *98*, 11623−11627.
(29) Lee, C.; Yang, W.; Parr, R. G. *Phys. Rev. B* **1988**, *37*, 785−789.
(30) Becke, A. D. *J. Chem. Phys.* **1993**, *98*, 5648−5652.
(31) Frisch, M. J.; et al. *Gaussian09*, Revision D.01; Gaussian, Inc.: Wallingford, CT, 2009.
(32) Cook, T. R.; Esswein, A. J.; Nocera, D. G. *J. Am. Chem. Soc.* **2007**, *129*, 10094−10095.
(33) Teets, T. S.; Lutterman, D. A.; Nocera, D. G. *Inorg. Chem.* **2010**, *49*, 3035−3043.
(34) Esswein, A. J.; Dempsey, J. L.; Nocera, D. G. *Inorg. Chem.* **2007**, *46*, 2362−2364.
(35) Andrae, D.; Haeussermann, U.; Dolg, M.; Stoll, H.; Preuss, H. *Theor. Chem. Acc.* **1990**, *77*, 123−141.
(36) Ditchfield, R.; Hehre, W. J.; Pople, J. A. *J. Chem. Phys.* **1971**, *54*, 724−728.
(37) Rassolov, V. A.; Ratner, M. A.; Pople, J. A.; Redfern, P. C.; Curtiss, L. A. *J. Comput. Chem.* **2001**, *22*, 976−984.
(38) Zhao, Y.; Truhlar, D. G. *Acc. Chem. Res.* **2008**, *41*, 157−167.
(39) Zhao, Y.; Truhlar, D. G. *Theor. Chem. Acc.* **2008**, *120*, 215−241.
(40) Zhao, Y.; Truhlar, D. G. *J. Chem. Phys.* **2006**, *125*, 194101.
(41) Reed, A. E.; Curtiss, L. A.; Weinhold, F. *Chem. Rev.* **1988**, *88*, 899−926.
(42) Weinhold, F.; Landis, C. R. *Valency and Bonding: A Natural Bond Orbital Donor−Acceptor Perspective*; Cambridge University Press: New York, 2005.
(43) Foster, J. P.; Weinhold, F. *J. Am. Chem. Soc.* **1980**, *102*, 7211−7218.
(44) Reed, A. F.; Weinstock, R. B.; Weinhold, F. *J. Chem. Phys.* **1985**, *83*, 735−746.
(45) Glendening, E.D.; Reed, A. E.; Carpenter, J. E.; Weinhold, F. *NBO*, version 3.1: University of Wisconsin: Madison, WI.
(46) Birkholz, M. *Thin Film Analysis by X-ray Scattering*; Wiley-VCH: Weinheim, Germany, 2006; p 183.
(47) Schmøkel, M. S.; Kamiński, R.; Benedict, J. B.; Coppens, P. *Acta Cryst. A* **2010**, *66*, 632−636.
(48) Parkin, G. *Struct. Bonding (Berlin, Ger.)* **2010**, *136*, 113−146.
(49) Green, M. L. H.; Parkin, G. *J. Chem. Educ.* **2014**, *91*, 807−816.
(50) Makal, A.; Benedict, J.; Trzop, E.; Sokolow, J.; Fournier, B.; Chen, Y.; Kalinowski, J. A.; Graber, T.; Henning, R.; Coppens, P. *J. Phys. Chem. A* **2012**, *116*, 3359−3365.
(51) Wickramasinghe, L. A.; Sharp, P. R. *Inorg. Chem.* **2014**, *53*, 1430−1442.
(52) Karikachery, A. R.; Lee, H. B.; Masjedi, M.; Ross, A.; Moody, M. A.; Cai, X.; Chui, M.; Hoff, C. D.; Sharp, P. R. *Inorg. Chem.* **2013**, *52*, 4113−4119.
(53) Lin, T.-P.; Gabbaï, F. P. *J. Am. Chem. Soc.* **2012**, *134*, 12230−12238.
(54) Carrera, E. I.; McCormick, T. M.; Kapp, M. J.; Lough, A. J.; Seferos, D. S. *Inorg. Chem.* **2013**, *52*, 13779−13790.
(55) Perera, T. A.; Masjedi, M.; Sharp, P. R. *Inorg. Chem.* **2014**, *53*, 7608−7621.
(56) Zheng, S.-L.; Wang, Y.; Yu, Z.; Lin, Q.; Coppens, P. *J. Am. Chem. Soc.* **2009**, *131*, 18036−18037.
(57) Cook, T. R.; Surendranath, Y.; Nocera, D. G. *J. Am. Chem. Soc.* **2009**, *131*, 28−29.
(58) Teets, T. S.; Nocera, D. G. *J. Am. Chem. Soc.* **2009**, *131*, 7411−7420.
(59) Yang, H.; Gabbaï, F. P. *J. Am. Chem. Soc.* **2014**, *136*, 10866−10869.
(60) Ohashi, Y. *Crystalline State Photoreactions: Direct Observation of Reaction Processes and Metastable Intermediates*; Springer: Tokyo, Japan, 2014.
(61) Coppens, P.; Zheng, S. L. In *Supramolecular Photochemistry: Controlling Photochemical Processes*; Ramamurthy, V., Inoue, T., Eds.; John Wiley & Sons: Hoboken, NJ, 2011; pp 155−175.
(62) Coppens, P.; Sokolow, J.; Trzop, E.; Makal, A.; Chen, Y. *J. Chem. Phys. Lett.* **2013**, *4*, 579−582.
(63) Makal, A.; Trzop, E.; Sokolow, J.; Kalinowski, J.; Benedict, J.; Coppens, P. *Acta Crystallogr., Sect. A* **2011**, *67*, 319−326.
(64) Benedict, J. B.; Makal, A.; Sokolow, J. D.; Trzop, E.; Scheins, S.; Henning, R.; Graber, T.; Coppens, P. *Chem. Commun.* **2011**, *47*, 1704−1706.

(65) Evans, J.; Okrasinski, S. J.; Pribula, A. J.; Norton, J. R. *J. Am. Chem. Soc.* **1977**, *99*, 5835−5836.
(66) Carter, W. J.; Okrasinski, S. J.; Norton, J. R. *Organometallics* **1985**, *4*, 1376−1386.
(67) Carter, W. J.; Kelland, J. W.; Okrasinski, S. J.; Warner, K. E.; Norton, J. R. *Inorg. Chem.* **1982**, *21*, 3955−3960.
(68) Wolczanski, P. T.; Threlkel, R. S.; Bercaw, J. E. *J. Am. Chem. Soc.* **1979**, *101*, 218−220.
(69) Janowicz, A. H.; Bergman, R. G. *J. Am. Chem. Soc.* **1981**, *103*, 2488−2489.
(70) Jones, W. D.; Huggins, J. M.; Bergman, R. G. *J. Am. Chem. Soc.* **1981**, *103*, 4415−4423.
(71) Nappa, M. J.; Santi, R.; Halpern, J. *Organometallics* **1985**, *4*, 34−41.
(72) Marsella, J. A.; Huffman, J. C.; Caulton, K. G.; Longato, B.; Norton, J. R. *J. Am. Chem. Soc.* **1982**, *104*, 6360−6368.
(73) Alemdaroğlu, N. H.; Penninger, J. L. M.; Oltay, E. *Monatsh. Chem.* **1976**, *107*, 1153−1165.
(74) Hebrard, F.; Kalck, P. *Chem. Rev.* **2009**, *109*, 4272−4282.
(75) Collman, J. P. *J. Organomet. Chem.* **1980**, *200*, 79−85.
(76) Liu, G.; Li, C.; Guo, L.; Garland, M. *J. Catal.* **2006**, *237*, 67−78.
(77) Feng, J.; Garland, M. *Organometallics* **1999**, *18*, 1542−1546.
(78) Mirbach, M. F. *J. Organomet. Chem.* **1984**, *265*, 205−213.
(79) Broussard, M. E.; Juma, B.; Train, S. G.; Peng, W.-J.; Laneman, S. A.; Stanley, G. G. *Science* **1993**, *260*, 1784−1788.
(80) Li, C.; Chen, L.; Garland, M. *J. Am. Chem. Soc.* **2007**, *129*, 13327−13334.
(81) Gray, T. G.; Veige, A. S.; Nocera, D. G. *J. Am. Chem. Soc.* **2004**, *126*, 9760−9768.